Cancer Letters 605 (2024) 217242

Contents lists available at ScienceDirect

Cancer Letters

journal homepage: www.elsevier.com/locate/canlet

Original Articles

Rewired glutamate metabolism diminishes cytostatic action of L-asparaginase

Katerina Hlozkova [a,b,**], Maryna Vasylkivska [a,b], Adam Boufersaoui [c], Bryan Marzullo [c], Matus Kolarik [a,b,d], Natividad Alquezar-Artieda [a,b], Mehak Shaikh [e], Nadia Fatemeh Alaei [a,b,e], Marketa Zaliova [a,b,f], Martina Zwyrtkova [a,b], Violeta Bakardijeva-Mihaylova [a,b], Meritxell Alberich-Jorda [a,b,e], Jan Trka [a,b,f], Daniel A. Tennant [c], Julia Starkova [a,b,f,*]

[a] Childhood Leukaemia Investigation Prague, Prague, Czech Republic
[b] Second Faculty of Medicine, Department of Pediatric Hematology and Oncology, Charles University, Prague, Czech Republic
[c] Institute of Metabolism and Systems Research, College of Medical and Dental Sciences, University of Birmingham, Birmingham, United Kingdom
[d] First Faculty of Medicine, Charles University, Prague, Czech Republic
[e] Laboratory of Hemato-Oncology, Institute of Molecular Genetics of the Czech Academy of Sciences, Prague, Czech Republic
[f] University Hospital Motol, Prague, Czech Republic

A B S T R A C T

Tumor cells often adapt to amino acid deprivation through metabolic rewiring, compensating for the loss with alternative amino acids/substrates. We have described such a scenario in leukemic cells treated with L-asparaginase (ASNase). Clinical effect of ASNase is based on nutrient stress achieved by its dual enzymatic action which leads to depletion of asparagine and glutamine and is accompanied with elevated aspartate and glutamate concentrations in serum of acute lymphoblastic leukemia patients. We showed that in these limited conditions glutamate uptake compensates for the loss of glutamine availability. Extracellular glutamate flux detection confirms its integration into the TCA cycle and its participation in nucleotide and glutathione synthesis. Importantly, it is glutamate-driven *de novo* synthesis of glutathione which is the essential metabolic pathway necessary for glutamate's pro-survival effect. *In vivo* findings support this effect by showing that inhibition of glutamate transporters enhances the therapeutic effect of ASNase. In summary, ASNase induces elevated extracellular glutamate levels under nutrient stress, which leads to a rewiring of intracellular glutamate metabolism and has a negative impact on ASNase treatment.

1. Introduction

Acute lymphoblastic leukemia (ALL) is the most prevalent cancer among children but it also affects adults [1]. Recent improvements in chemotherapy and supportive care have resulted in complete remission rates of about 98 % for children and about 85 % for adults after induction therapy [2]. However, overall survival is only reaching 80–85 % for pediatric and 50 % for adult ALL patients [3–5], mainly due to the resistance to current treatment options. Management of drug resistance and prevention of disease relapse thus still remain the biggest challenges for successful treatment [6,7].

L-asparaginase (ASNase) has been part of the first-line therapy for almost 50 years now. Despite the undeniable benefit of intensive ASNase treatment [8,9], its complete mechanism of action still eludes comprehensive understanding. ASNase transforms extracellular asparagine and glutamine to aspartate and glutamate, respectively, and we have previously shown that ASNase reprogrammed the metabolism of leukemia cells both *in vitro* [10] and *in vivo* [11]. The discoveries emphasized the importance of asparagine and glutamine dependence while aspartate and/or glutamate were not considered in this ASNase-driven action. Until now, high aspartate and glutamate extracellular concentrations have been considered to only be a by-product of ASNase treatment without any known consequences. Notably, the levels of intracellular glutamate and aspartate modulate crucial biological processes [12,13]. Given the above, we investigated the role of aspartate and glutamate in the process of metabolic adaptation of lymphoblasts to ASNase treatment. Better understanding of downstream metabolic consequences of ASNase treatment could help to uncover possible adverse mechanisms.

* Corresponding author. Childhood Leukaemia Investigation Prague, Prague, Czech Republic.
** Corresponding author. Childhood Leukaemia Investigation Prague, Prague, Czech Republic.
E-mail addresses: katerina.hlozkova@lfmotol.cuni.cz (K. Hlozkova), julia.starkova@lfmotol.cuni.cz (J. Starkova).

https://doi.org/10.1016/j.canlet.2024.217242
Received 13 March 2024; Received in revised form 2 September 2024; Accepted 6 September 2024
Available online 11 September 2024

2. Results

2.1. Leukemia cells express aspartate and glutamate transporters

The use of extracellular aspartate and/or glutamate by leukemic cells is dependent on their uptake. Therefore, we first decided to measure the expression of genes encoding aspartate and glutamate transporters in leukemic cells. So far, no information about its expression in leukemia cells has been published. We decided to measure not only the expression of SLC1A3, the most studied aspartate and glutamate transporter in tumors [14–18], but also expression of the other members of SLC1 family that are able to transport aspartate and glutamate (SLC1A1, SLC1A2, SCL1A6 and SLC1A7). First, we focused on ALL cell lines. The qPCR results revealed that all six cell lines tested (B-ALL: NALM6, REH, RS4;11, SUP-B15; T-ALL: JURKAT, MOLT4) expressed transcripts encoding aspartate and glutamate transporters, although each cell line expressed a different set of transporters (Fig. 1A). As expected, SLC1A3 was the most broadly expressed compared to other transporters genes, while SLC1A7 was undetectable (data not shown) in any of the tested cell lines. Next, using RNAseq data from diagnostic samples of acute leukemia patients, we determined whether these transcripts were also expressed in primary cells. The results showed SLC1A3 and, surprisingly, SLC1A7, being the most expressed ones not only in BCP-ALL and T-ALL but also in AML patients (Fig. 1B). However, other genes coding for aspartate and glutamate transporters were also expressed. Taken together, these results demonstrated that leukemia cells express genes coding for aspartate and glutamate transporters, indicating that these cells could be able to transport aspartate and/or glutamate.

2.2. Leukemia cells transport aspartate and glutamate from the media

Glucose and glutamine are the most important nutrients fueling TCA cycle since they quantitatively account for the majority of TCA cycle carbons (Fig. S1A) [19]. Importantly, since ASNase's dual enzymatic activity also results in depletion of glutamine, which replenishes TCA cycle and directly affects aspartate and glutamate levels, we investigated TCA cycle changes induced by ASNase treatment (resulting in asparagine and glutamine depletion and aspartate and glutamate elevation) versus by isolated glutamine withdrawal. We observed that glutamine depletion alone (glutamine-free RPMI) reduced the abundance of TCA cycle metabolites in ALL cells (Fig. S1B-D). Moreover, intracellular concentrations of aspartate and glutamate, two amino acids directly derived from TCA cycle intermediates, were also significantly decreased after glutamine removal from the media (Fig. S1E,F). Consistent with the increased extracellular availability of aspartate and glutamate upon treatment of cells with ASNase, we did not detect decrease in intracellular aspartate and glutamate concentrations that we observed in glutamine-free RPMI medium (Fig. S1G,H). One possible explanation could be that cells replenish their intracellular aspartate and glutamate pools by transporting aspartate and glutamate from the media, respectively. To investigate that, we cultured NALM6 and REH B-ALL cell lines for 24 h in full RPMI, RPMI without asparagine and glutamine with standard aspartate and glutamate concentrations, and RPMI without asparagine and glutamine with increased aspartate and glutamate concentrations (corresponding to those after ASNase treatment). In every tested condition, either aspartate or glutamate was replaced by its isotopically labeled analog ($^{13}C_4$-aspartate or $^{13}C_5$-glutamate) which was then traced inside the cells (Fig. 1C). The results showed that both tested cell lines were able to import aspartate and glutamate from the media in a dose-dependent manner since we were able to detect both intracellular M4 aspartate (Fig. 1D) and M5 glutamate (Fig. 1E).

2.3. Glutamate enhances survival of leukemia cells after ASNase treatment

Next, we asked whether glutamate and/or aspartate uptake was mechanistically important to leukemic cells survival after ASNase. Therefore, we cultivated the cells in four different media: 1) RPMIØ (RPMI without asparagine, glutamine, aspartate and glutamate); 2) RPMIØ+Asp; 3) RPMIØ+Glu; 4) RPMIØ+Asp+Glu (Fig. 1F). Altogether, we tested five ALL cell lines (REH, MOLT4, NALM6, SUP-B15 and RS4;11). Cells were cultured for 72, 96 and 120 h, then, their survival was measured using absolute count on flow cytometry. We observed that, after 120 h, aspartate alone did not have any effect on cell growth compared to cells cultured in RPMIØ, or only showed minor effects on cell survival (Fig. 1G). However, the survival of four out of five cell lines tested was significantly enhanced when glutamate was present in the media (Fig. 1G, S2A). The combination of aspartate and glutamate did not have any additional effect compared to glutamate only (Fig. 1G). Of note, similar trends were observed after 72 and 96 h of cultivation (Figs. S2B,C). To corroborate the effect of glutamate in unperturbed conditions, or after ASNase, MOLT4 cell line was cultivated in RPMIØ and in RPMIØ with increasing glutamate concentrations (Fig. 1F, S2D). The results confirmed positive effects of after-ASNase-glutamate concentration on leukemia cell survival (Fig. S2D). Overall, the results revealed interesting phenomenon, in which leukemia cells survival under asparagine- and glutamine-depleted conditions is boosted by extracellular glutamate, but not aspartate.

2.4. Glutamate boosts TCA cycle in leukemia cells after ASNase treatment

We next explored how glutamate uptake was able to support leukemic cells survival under ASNase-like conditions. To mechanistically examine whether intracellular glutamate derived from direct uptake contributed to catabolic fates, such as TCA cycle anaplerosis, we leveraged stable isotope tracing with $^{13}C_5$-glutamate. More explicitly, we measured the incorporation of $^{13}C_5$-glutamate from the media into TCA cycle intermediates (Fig. 2A), cultivating leukemia cell lines for 24 h in full RPMI, RPMIØ+GluA (after-ASNase glutamate; 1.136 mM calculated as all glutamine is converted to glutamate (1 mM) plus 0.136 mM glutamate that full RPMI contains) and RPMIØ+Glu (Fig. 1F), where (in each medium) glutamate was replaced by $^{13}C_5$-glutamate. The results from all tested cell lines showed that, under RPMIØ+GluA and RPMIØ+Glu conditions, $^{13}C_5$-glutamate is metabolized to α-KG and then further into TCA cycle intermediates (Fig. 2B,C, S3A,B). In full RPMI, as expected, $^{13}C_5$-glutamate incorporated into the TCA cycle only marginally (Fig. 2B,C, S3A,B), due to glutamine being the major anaplerotic substrate when glutamine present [20]. Altogether, our results revealed a metabolic rewiring mechanism after ASNase treatment with glutamate replacing glutamine in the context of anaplerosis. TCA cycle boost from glutamate on RPMIØ background could explain its pro-survival effect. However, in RS4;11, the only cell line which survival was not augmented by glutamate under RPMIØ condition, glutamate was still used to boost TCA cycle (Fig. 2B,C, S3A,B). Therefore, this alternative anaplerosis is not sufficient on its own to increase post-ASNase cell survival in some instances.

Importantly, glucose also contributes as a substrate to the TCA cycle (Fig. 2D) [21]. To determine the role of glucose in glutamate-driven survival under RPMIØ conditions, we cultivated leukemia cell lines for 24 h in RPMIØ and RPMIØ+Glu where (in both media) glucose was replaced by $^{13}C_6$-glucose. In all tested cell lines, we detected higher glucose contribution to aspartate, glutamate and TCA cycle intermediates (both M2 and M3) in RPMIØ+Glu compared to RPMIØ (Fig. 2E,F, S3C,D). Moreover, we also observed glutamate-driven switch from fermentation to oxidative metabolism as we detected higher abundance of M3 pyruvate and lower of M3 lactate in RPMIØ+Glu compared to RPMIØ (Figs. S3E and F). Overall, our data unraveled rewired glucose metabolism upon glutamate addition to RPMIØ indicating that glucose plays a non-negligible role in glutamate-driven survival.

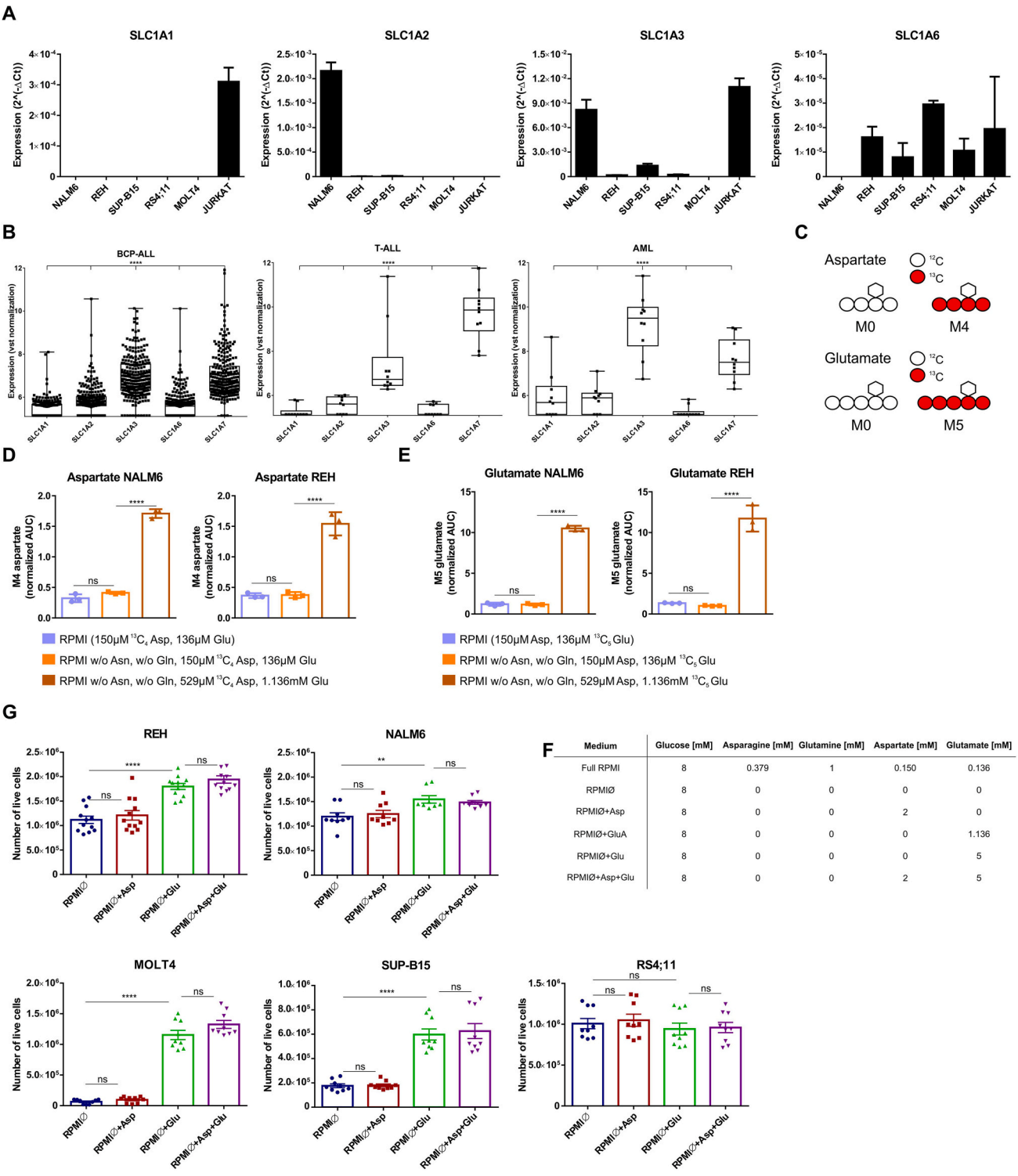

F

Medium	Glucose [mM]	Asparagine [mM]	Glutamine [mM]	Aspartate [mM]	Glutamate [mM]
Full RPMI	8	0.379	1	0.150	0.136
RPMIØ	8	0	0	0	0
RPMIØ+Asp	8	0	0	2	0
RPMIØ+GluA	8	0	0	0	1.136
RPMIØ+Glu	8	0	0	0	5
RPMIØ+Asp+Glu	8	0	0	2	5

Fig. 1. Leukemia cells uptake glutamate which then affects their survival under asparagine- and glutamine-depleted conditions
(A) Expression of genes coding for aspartate/glutamate transporters SLC1A1, SLC1A2, SLC1A3 and SLC1A6 in six ALL cell lines. Measured by RT-PCR with *ABL1* and *β2-microglobuline* as reference genes. n = 9 presented as mean ± SD. **(B)** Expression of genes coding for aspartate/glutamate transporters SLC1A1, SLC1A2, SLC1A3, SLC1A6 and SLC1A7 in primary leukemia cells from pediatric patients diagnosed with BCP-ALL, T-ALL an AML. Measured by RNAseq with vst normalization. n = 262 for BCP-ALL, n = 10 for T-ALL and AML presented with mean, min and max. **(C)** Uniformly labeled aspartate ($^{13}C_4$-aspartate) and glutamate ($^{13}C_5$-glutamate). **(D)** Intracellular relative M4 aspartate abundance (peak area normalized to internal standard and cell number) measured by GC/MS in NALM6 and REH. $^{13}C_4$-aspartate was used as a tracer. n = 3 presented as mean ± SD. **(E)** Intracellular relative M5 glutamate abundance (peak area normalized to internal standard and cell number) measured by GC/MS in NALM6 and REH. $^{13}C_5$-glutamate was used as a tracer. n = 3 presented as mean ± SD. **(F)** Composition of media further used in the study. **(G)** Growth of REH, NALM6, MOLT4, SUP-B15 and RS4;11 cell lines after 120 h-long culture in different conditions measured by absolute count on flow cytometry. n = 9 presented as mean ± SEM.

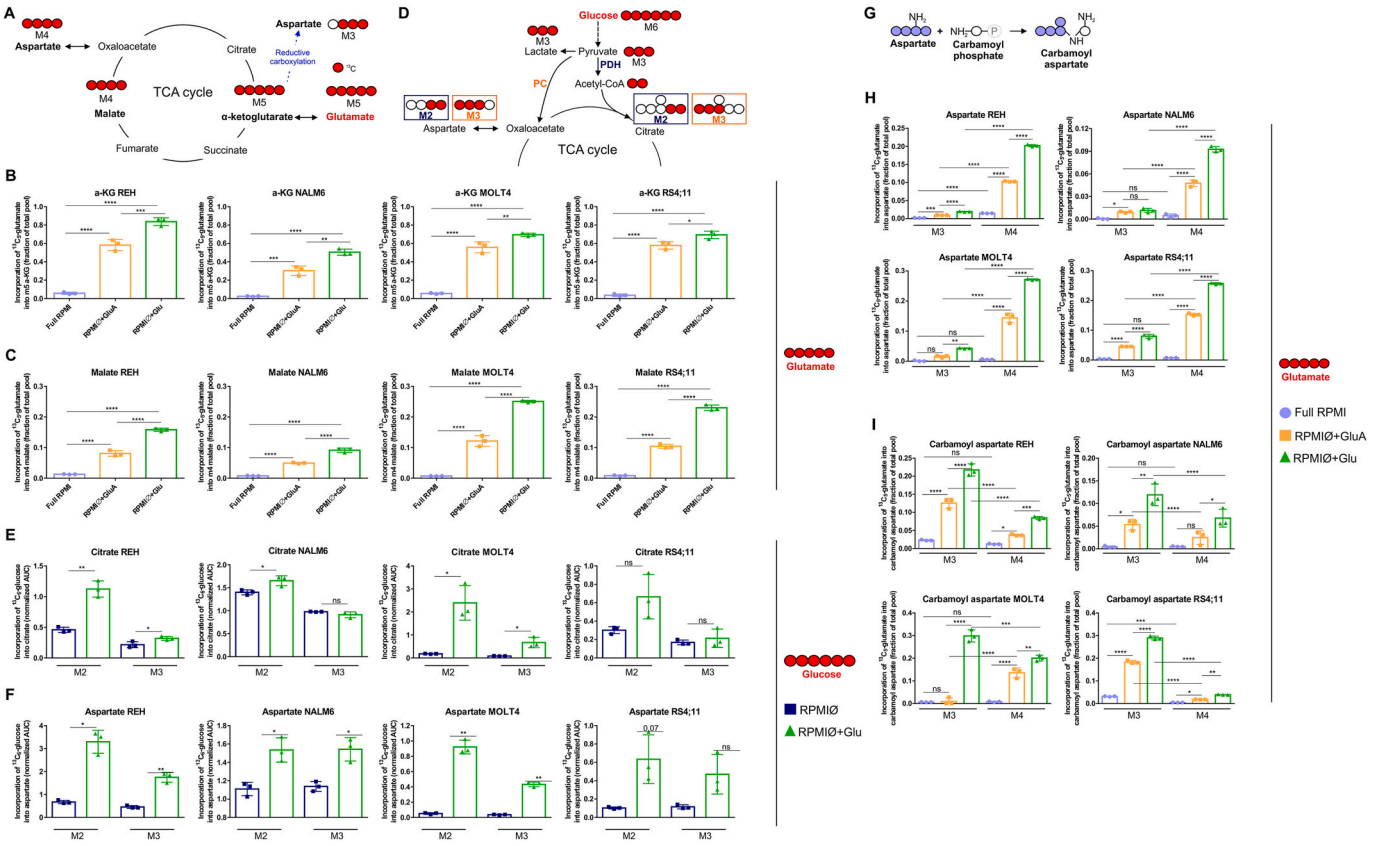

Fig. 2. Glutamate rewires leukemia cell metabolism under asparagine- and glutamine-depleted conditions
(A) Diagram showing $^{13}C_5$-glutamate entry and incorporation into TCA cycle and aspartate. **(B)** Incorporation of $^{13}C_5$-glutamate into α-KG in REH, NALM6, MOLT4 and RS4;11 cells. Results are presented as M5 proportion from total pool measured by GC/MS. n = 3 presented as mean ± SD. **(C)** Incorporation of $^{13}C_5$-glutamate into malate in REH, NALM6, MOLT4 and RS4;11 cells. Results are presented as M4 proportion from total pool measured by GC/MS. n = 3 presented as mean ± SD. **(D)** Diagram showing $^{13}C_6$-glucose metabolism emphasizing differences between fermentation and oxidative metabolism. **(E)** Incorporation of $^{13}C_6$-glucose into citrate in REH, NALM6, MOLT4 and RS4;11 cells. Results are presented as M2 and M3 relative abundances (peak area normalized to internal standard and cell number) measured by GC/MS. n = 3 presented as mean ± SD. **(F)** Incorporation of $^{13}C_6$-glucose into aspartate in REH, NALM6, MOLT4 and RS4;11 cells. Results are presented as M2 and M3 relative abundances (peak area normalized to internal standard and cell number) measured by GC/MS. n = 3 presented as mean ± SD. **(G)** Diagram showing the first step in pyrimidine biosynthesis: formation of carbamoyl aspartate from aspartate and carbamoyl phosphate. **(H)** Incorporation of $^{13}C_5$-glutamate into aspartate in REH, NALM6, MOLT4 and RS4;11 cells. Results are presented as M3 and M4 proportions from total pool measured by LC/MS. n = 3 presented as mean ± SD. **(I)** Incorporation of $^{13}C_5$-glutamate into carbamoyl aspartate in REH, NALM6, MOLT4 and RS4;11 cells. Results are presented as M3 and M4 proportions from total pool measured by LC/MS. n = 3 presented as mean ± SD.

2.5. Glutamate is used for nucleotide biosynthesis in leukemia cells after ASNase treatment

To get more insight into glutamate-driven survival under RPMIØ conditions, we explored the possibility that glutamate could be also used as a precursor for nucleotide synthesis. Therefore, we measured the incorporation of $^{13}C_5$-glutamate into aspartate and carbamoyl aspartate (Fig. 2A,G), established intermediates of pyrimidine biosynthesis pathway [22], and then further into UMP, CTP and dTTP. We cultivated leukemia cell lines for 24 h in full RPMI, RPMIØ+GluA and RPMIØ+Glu (Fig. 1F) where (in all three media) glutamate was replaced by $^{13}C_5$-glutamate. In full RPMI, label incorporation into aspartate or carbamoyl aspartate was almost undetectable (Fig. 2H and I). However, when cells were cultured in RPMIØ+GluA or RPMIØ+Glu, we observed that glutamate was metabolized to aspartate and subsequently carbamoyl aspartate (Fig. 2H and I). A similar trend was observed in UMP, CTP and dTTP metabolites (Figs. S4A–C). Of note, most aspartate was produced from glutamate via oxidative TCA cycle activity, as we detected significantly higher proportion of M4 aspartate compared to that of M3 aspartate. On the other hand, we detected higher proportion of M3 carbamoyl aspartate compared to that of M4 carbamoyl aspartate (Fig. 2H and I), implying the preference of reductive-carboxylation-originated aspartate for pyrimidine biosynthesis from glutamate. Thus, we conclude that under asparagine- and glutamine-depleted conditions and elevated glutamate levels, leukemia cells can support the carbon requirement for nucleotide biosynthesis.

2.6. Glutamate increases ROS in leukemia cells after ASNase treatment

A major source of ROS within the cell is mitochondrial respiration where ROS are generated as its by-product [23,24]. We detected reduced TCA cycle intermediates in RPMIØ compared to full RPMI (Fig. S5A-C), which indicates that the respiration is likely reduced under RPMIØ conditions. However, in the presence of glutamate at elevated levels, the TCA cycle was replenished (Fig. 2B,C, S3A,B) suggesting increased respiration and, consequently, ROS production. We measured intracellular ROS levels in leukemia cells cultivated in four different media: 1) RPMIØ; 2) RPMIØ+Asp; 3) RPMIØ+Glu; 4) RPMIØ+Asp+Glu (Fig. 1F). In all cell lines tested, the results showed increased ROS levels after 72 h culture in RPMIØ+Glu compared to RPMIØ (Fig. 3A). 24- and 48-h cultivation increased ROS levels in three out of five cell lines tested indicating cell line-specific velocity of ROS management (Fig. S5D,E). Aspartate addition to RPMIØ did not affect intracellular ROS levels and combination of aspartate and glutamate had no further effect (Fig. 3A,

S5D,E). Altogether, these results demonstrate that after ASNase treatment, glutamate but not aspartate increases ROS production, which likely contributes to its post-ASNase pro-survival effect.

2.7. Glutamate is used for GSH biosynthesis in leukemia cells after ASNase treatment

Inadequate ROS generation has been recognized as a mechanism by which mitochondrial dysfunction leads to apoptosis [25]. Interestingly, our data suggest that ROS production upon glutamate rewiring is part of survival mechanism after ASNase treatment (Figs. 1G and 3A). To explain this discrepancy, we hypothesized that induction of a ROS scavenging mechanism could mitigate the excess ROS produced. An ideal candidate for such a scavenger would be GSH since it is the most abundant cell antioxidant and, importantly, glutamate is required for synthesis of this tripeptide [26]. First, we looked into total GSH level in leukemia cells cultivated for 24 h in four different media: 1) RPMIØ; 2) RPMIØ+Asp; 3) RPMIØ+Glu; 4) RPMIØ+Asp+Glu (Fig. 1F). The results revealed that in MOLT4 and SUP-B15 cell lines, total GSH level was increased in cells cultivated in RPMIØ+Glu compared to RPMIØ (Fig. 3B). The same trend was observed in REH cell line. Unexpectedly, in NALM6 cell line (also rescued by glutamate in RPMIØ conditions), we detected a minor but significant decrease in total GSH level in cells cultivated in RPMIØ+Glu compared to RPMIØ (Fig. 3B). In RS4; 11, the cell line in which survival was not induced by the addition of glutamate to RPMIØ, we detected similar total GSH levels in cells cultivated in RPMIØ and RPMIØ+Glu (Fig. 3B). In all cell lines tested, aspartate addition to RPMIØ did not have any effect on total GSH level. The combination of aspartate and glutamate did not have any additional effect compared to glutamate only (Fig. 3B).

The increase in total GSH observed in those cell lines whose viability was supported by exogenous glutamate suggests that this amino acid may be used for GSH biosynthesis under these conditions. To evaluate this hypothesis, we measured the incorporation of $^{13}C_5$-glutamate from the media into *de novo* synthesized GSH (detected as M5 GSH, Fig. 3C), and found that after 24 h in full RPMI, RPMIØ+GluA and RPMIØ+Glu (Fig. 1F) containing $^{13}C_5$-glutamate, there was considerable $^{13}C_5$-glutamate incorporation into *de novo* synthesized GSH in both RPMIØ+GluA and RPMIØ+Glu compared to full RPMI (Fig. 3D). Surprisingly, we detected M5 GSH also in RS4;11 cell line (Fig. 3D), which survival was not enhanced by glutamate addition into RPMIØ. Of note, when we treated the cells cultured in RPMIØ+Glu with vitamin E (ROS scavenger), neither $^{13}C_5$-glutamate incorporation into GSH was affected nor $^{13}C_5$-glutamate uptake (Fig. 3D, S6A,B). This supports glutamate-derived biosynthesis of GSH not being ROS-induced phenomenon. Notably, GSH biosynthesis from glutamate itself was not generally sufficient to maintain or increase the total GSH pool (NALM6 and RS4;11; Fig. 3B). This abundance differences could be partially explained in NALM6, where isotopic enrichment of GSH from $^{13}C_5$-glutamate was only half of the enrichment of REH, MOLT4 and RS4;11 cell lines.

2.8. GSH biosynthesis from glutamate is crucial for leukemia cells after ASNase treatment

To assess the importance of *de novo* GSH synthesis for cells cultured in RPMIØ+Glu, we inhibited this pathway with BSO (buthionine sulphoximine; Fig. 3C), and compared the changes in intracellular ROS levels in leukemia cells cultivated for 24 h in RPMIØ, RPMIØ+Glu and full RPMI. In REH and SUP-B15 cell lines, treating the cells with increasing concentrations of BSO resulted in a steeper ROS increase in RPMIØ+Glu compared to both RPMIØ and full RPMI (Fig. 3E). In NALM6, ROS increase was also the steepest in RPMIØ+Glu but the change in RPMIØ was higher than in full RPMI (Fig. 3E). The MOLT4 cell line was the most resistant to BSO amongst all tested cell lines (Fig. S6C). Treating this cell line with BSO resulted in a significant increase in ROS level when cells were cultivated in both RPMIØ and RPMIØ+Glu (Fig. 3E). On the other hand, only a minor change in ROS level was detected when MOLT4 cells were cultivated in full RPMI. It is not clear why the change in ROS level was similar in MOLT4 cells in both RPMIØ and RPMIØ+Glu media, but it may be attributed to their high level of resistance to BSO together with their relatively high expression of enzymes related to GSH biosynthesis and recycling pathways compared to other tested cell lines (Fig. S6D). In RS4;11, the only cell line which survival is not augmented by glutamate addition to RPMIØ, we detected a much less profound change of ROS level after BSO treatment compared to other cell lines (Fig. 3E).

Our results indicate that the GSH biosynthesis supported in RPMIØ+Glu medium is crucial for leukemia cells. However, we wished to test whether this mechanism was responsible for support of cell survival in these conditions? We therefore cultivated NALM6 cells in RPMIØ and RPMIØ+Glu and we treated them with BSO and/or vitamin E. We found that BSO inhibited the growth of the cells cultivated in RPMIØ+Glu to a much greater extent compared to those in RPMIØ, with the effect of BSO completely reversed by vitamin E (Fig. 3F). These results further confirmed our hypothesis: that GSH biosynthesis from glutamate under asparagine- and glutamine-depleted conditions is essential for leukemia cell survival.

2.9. Primary leukemia cells are affected by glutamate after ASNase treatment

Finally, we sought to validate our observations in primary leukemic cells. Since we have shown aspartate/glutamate transporters being expressed in primary cells (Fig. 1B), we wanted to confirm that primary leukemia cells can also transport glutamate from the extracellular environment. We cultured primary leukemia cells from three patients at the time of diagnosis for 24 h in full RPMI, RPMIØ+GluA and RPMIØ+Glu where (in all three media) glutamate was replaced by $^{13}C_5$-glutamate which was then traced inside the cells (Fig. 1C). The results showed that all three patients tested were able to import glutamate from the media in a dose-dependent manner as we were able to detect intracellular M5 glutamate (Fig. 4A, S7A). Next, to verify glutamate-driven survival in primary leukemia cells, we cultured them in RPMIØ, RPMIØ+GluA and RPMIØ+Glu for 120 h, and the number of viable cells was determined. We observed that the survival of primary leukemia cells from two out of three patients was significantly enhanced with glutamate added into RPMIØ (Fig. 4B). We also sought to test whether the metabolism of glutamate in these conditions was similar to that observed in the cell line models. We noted that in full RPMI, $^{13}C_5$-glutamate was incorporated into aspartate and TCA cycle only marginally (Fig. 4C–E), while under RPMIØ+GluA and RPMIØ+Glu conditions, $^{13}C_5$-glutamate was metabolized to α-KG and then further into TCA cycle intermediates and aspartate (Fig. 4C–E). Altogether, we demonstrated that glutamate-driven survival under RPMIØ conditions applied to primary leukemia cells, where imported glutamate also entered TCA cycle. These results further emphasize the importance of glutamate in mitigating the cytostatic effect of ASNase.

2.10. Sensitivity to ASNase is altered by glutamate uptake inhibition in vivo

Could this newly described dichotomous effect of ASNase on cellular survival be potentially utilized in leukemia therapy? To explore this attractive possibility, we established a mouse NALM6-xenograft model, in which they were treated either with ASNase, TFB-TBOA (inhibitor of aspartate/glutamate transporters) or the combination of these two drugs (Fig. S7B). Weight of animals was not changed in any of the group tested (Fig. S7C). Our hypothesis was that, by inhibiting glutamate uptake, leukemia burden of leukemia-bearing mice after ASNase treatment would be reduced. It has been demonstrated that spleen size is increased in leukemic compared to non-leukemic mice [27] and that spleen weight positively correlates with tumor burden [28]. As shown at Fig. 4F and

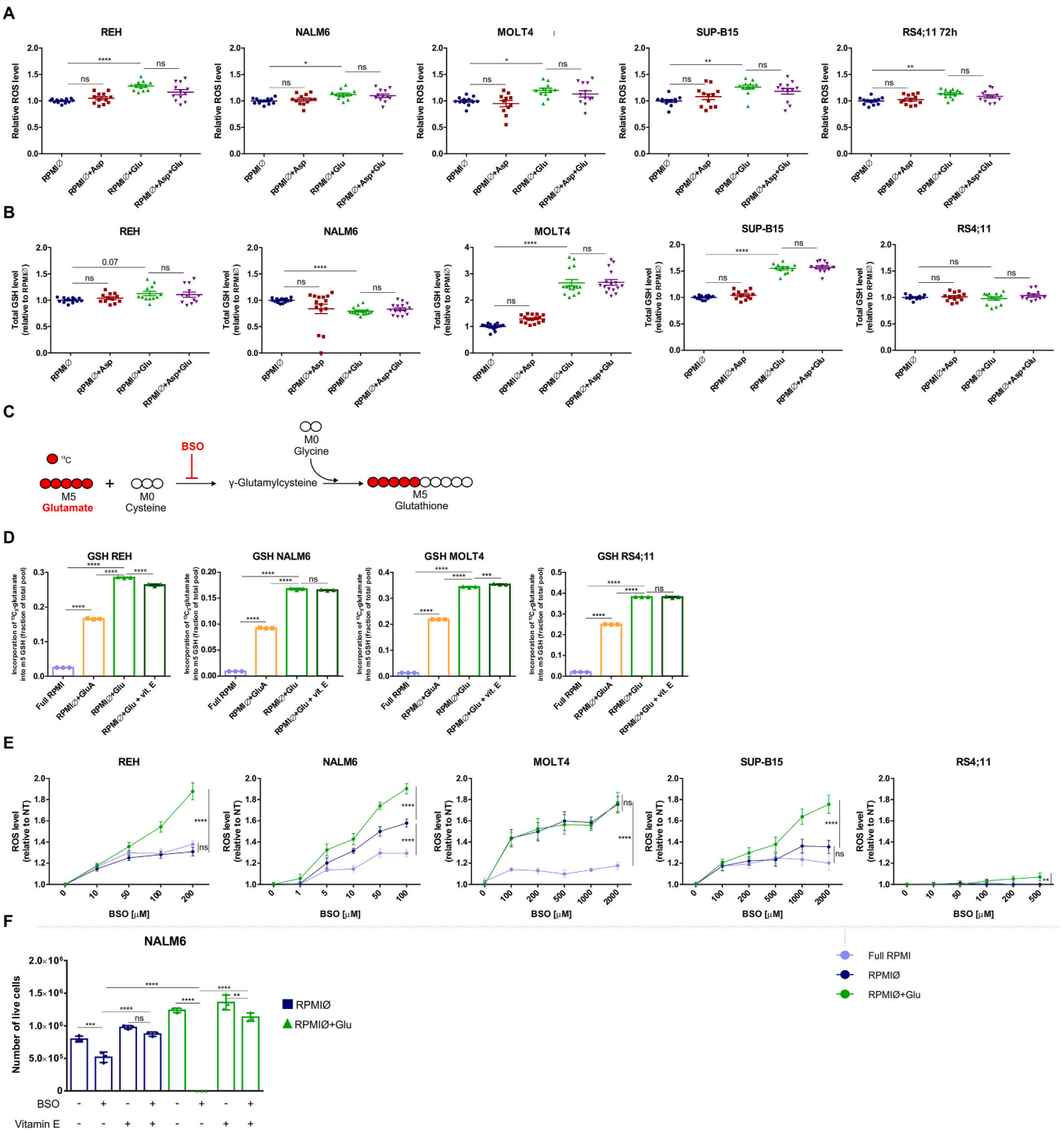

Fig. 3. Glutamate influences redox homeostasis under asparagine- and glutamine-depleted conditions
(A) Intracellular ROS levels after 72 h-long culture in different conditions normalized to RPMIØ in REH, NALM6, MOLT4, SUP-B15 and RS4;11 cells. n = 12 presented as mean ± SEM. **(B)** Intracellular total GSH level after 24 h-long culture in different conditions normalized to RPMIØ in REH, NALM6, MOLT4, SUP-B15 and RS4;11 cells. n = 15 presented as mean ± SEM. **(C)** Diagram showing $^{13}C_5$-glutamate incorporation into GSH. **(D)** Incorporation of $^{13}C_5$-glutamate into GSH (as its NEM-derivative) in REH, NALM6, MOLT4 and RS4; 11 cells. Results are presented as M5 proportion from total pool measured by LC/MS. Vitamin E treatment was 100 μM. n = 3 presented as mean ± SD. **(E)** Intracellular ROS levels after 24 h-long culture in different conditions together with BSO treatment with indicated concentrations normalized to NT controls in REH, NALM6, MOLT4, SUP-B15 and RS4; 11 cells. n = 9 presented as mean ± SEM. **(F)** Growth of NALM6 cells after 120 h-long culture in RPMIØ and RPMIØ+Glu with indicated treatment with BSO (10 μM) and vitamin E (100 μM) measured by absolute count on flow cytometry. n = 3 presented as mean ± SD.

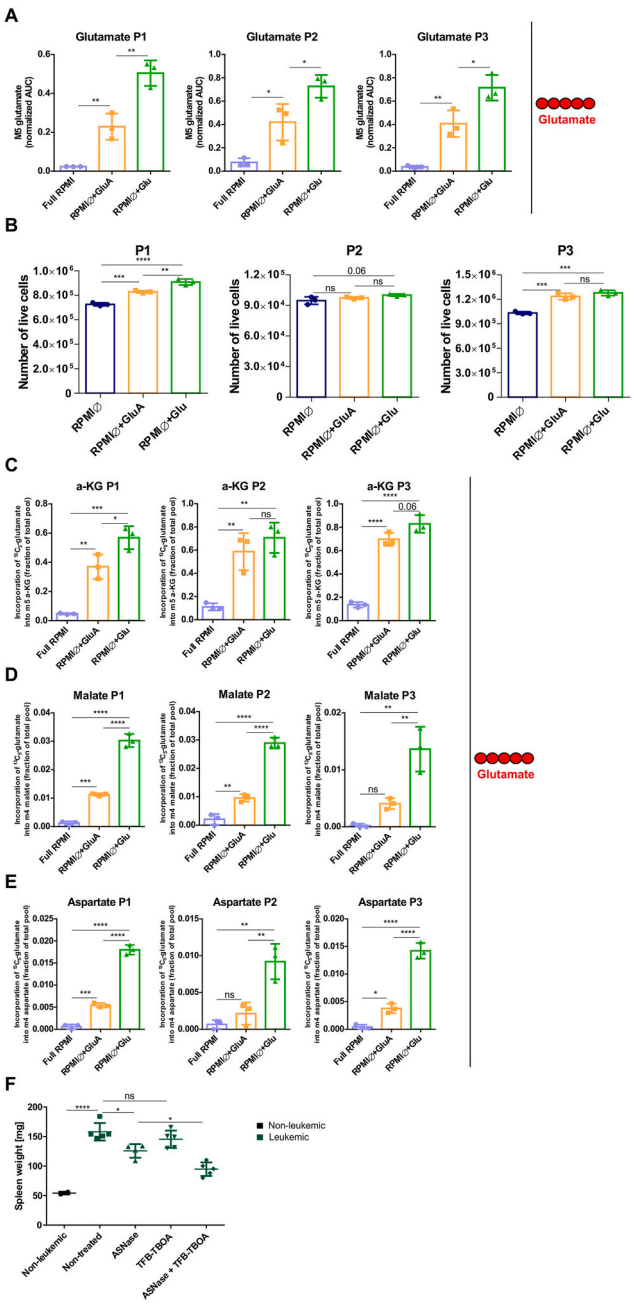

Fig. 4. Glutamate affects survival and metabolism of primary leukemia cells under asparagine- and glutamine-depleted conditions

(A) Intracellular M5 glutamate proportion from total pool in primary leukemia cells from three different patients measured by GC/MS. $^{13}C_5$-glutamate was used as a tracer. n = 3 presented as mean ± SD. **(B)** Growth of primary leukemia cells from three different patients after 120 h-long culture in different conditions measured by absolute count on flow cytometry. n = 3 presented as mean ± SD. **(C)** Incorporation of $^{13}C_5$-glutamate into α-KG in primary leukemia cells from three different patients. Results are presented as M5 proportion from total pool measured by GC/MS. n = 3 presented as mean ± SD. **(D)** Incorporation of $^{13}C_5$-glutamate into malate in primary leukemia cells from three different patients. Results are presented as M4 proportion from total pool measured by GC/MS. n = 3 presented as mean ± SD. **(E)** Incorporation of $^{13}C_5$-glutamate into aspartate in primary leukemia cells from three different patients. Results are presented as M4 proportion from total pool measured by GC/MS. n = 3 presented as mean ± SD. **(F)** Spleen weight of NALM6-xenograft mouse model treated with either ASNase, or TFB-TBOA or their combination. Non-leukemic: n = 2, non-treated: n = 5, ASNase: n = 4; TFB-TBOA: n = 5, ASNase + TFB-TBOA: n = 5; data are presented as mean ± SD.

S7D, spleen weight in leukemic mice was significantly increased compared to non-leukemic mice. ASNase treatment decreased the spleen weight, consistent with reduced tumor burden. Inhibiting glutamate uptake by TFB-TBOA alone did not change the weight of the spleen (Fig. 4F). However, the combination of ASNase with TFB-TBOA significantly reduced the spleen weight compared to single agent-treated mice (Fig. 4F). Nevertheless, changes in spleen size were not accompanied by changes in cellularity (Fig. S7E). Altogether, our results show that therapeutic effect of ASNase can be potentiated by the inhibition of glutamate uptake *in vivo*.

3. Discussion

The enzymatic activity of ASNase results in the depletion of asparagine and glutamine, with a consequent increase in extracellular levels of aspartate and glutamate. The cytotoxic effect of ASNase is mainly attributed to the deprivation of asparagine and glutamine and the cells' response to this deficiency. The role of glutamate and aspartate, by-products of the drug, has been overlooked in this context. One of the reasons why these amino acids were not considered in the action is that their transport has traditionally been described only in brain cells [29,30]. This has been recently challenged by Sun et al. [18] who published that certain solid tumors expressed the aspartate and glutamate transporter SLC1A3. Furthermore, the knockout of this transporter increased the sensitivity of the cells to ASNase; whereas the addition of cell-permeable aspartate or glutamate revoked the knockout effect. Since this scenario has not yet been pursued in leukemic cells, we firstly determined the expression of SLC1A3 and other aspartate and transporters in leukemic cells. We confirmed that leukemic cells expressed genes encoding aspartate and glutamate transporters including SLC1A3. Transporters differed among leukemia subtypes and, moreover, cell lines preferentially expressed different transporters compared to primary cells. Tracing results confirmed that both aspartate and glutamate were transported into leukemia cells in a dose dependent manner. Importantly, transported glutamate but not aspartate augmented leukemic cell survival under asparagine and glutamine-deprived conditions. Recently, it has been demonstrated that aspartate is a metabolic limitation for tumor cell survival [31,32]. Furthermore, aspartate synthesis has been demonstrated as crucial for proliferating cells [33]. On the other hand, the role of glutamate in tumor survival has not yet been demonstrated [34]. Interestingly, remarkable rescue effect seen in MOLT4 and SUP-B15 cell lines cannot be explained only by different expression of aspartate/glutamate transporters. We observed higher glutamate uptake in MOLT4 cells compared to NALM6 and REH, indicating either existence of other, not tested transporters, or independence between transporters expression and uptake rate.

We further showed that simultaneous asparagine- and glutamine-deprived conditions altered glutamate metabolism in leukemia cells, presumably glutamine depletion being responsible to trigger glutamate rewiring and its utilization in certain metabolic processes. Glutamine is considered conditionally essential in cancer cells, playing a key role in cellular metabolism [35]. It provides a pool of α-KG to fuel TCA cycle to generate ATP and supplies carbon and nitrogen to fuel biosynthesis. Cells cannot survive without glutamine, but there are some amino acids that are able to partially replace its function [36]. One of them is asparagine, which is, however, depleted as well upon ASNase treatment. Up until now, there is no evidence indicating that glutamate has the ability to compensate for glutamine deprivation. Our observations revealed that, under simultaneous asparagine- and glutamine-depleted conditions, glutamate boosts TCA cycle and participates in nucleotide biosynthesis. Under the same conditions, glutamate increases also intracellular ROS levels. The role of ROS in biological systems is entirely dependent on the context [37]. By boosting the TCA cycle under asparagine- and glutamine-depleted conditions, glutamate provides the electrons to support respiratory chain activity, leading to ROS production. Increased oxidative stress thus results in a drive for additional

glutathione biosynthesis. Hence, based on our results, we propose that the glutamate available as a result of ASNase treatment elicits pro-survival mechanisms in two interlinked metabolic processes. However, although we showed various fates of imported glutamate, the regulation and interconnection between TCA cycle anaplerosis and GSH biosynthesis still remain elusive. A few other studies have also observed a relationship between TCA cycle activity and redox state of the different types of cells [38,39]. Noteworthy, inhibition of glutathione synthesis results in increased ROS levels in all tested cell lines and to reduced survival of NALM6 cells provided with glutamate under asparagine- and glutamine-depleted conditions. Moreover, pharmacological inhibition of aspartate and glutamate transporters mitigates sensitivity to ASNase *in vivo*. However, while we are suggesting a potential therapeutic opportunity through this pharmacological intervention, it is essential that this possibility is addressed in a more detailed study.

We did not observe glutamate-driven survival advantage under asparagine- and glutamine-depleted conditions in only one cell line tested – RS4;11. Surprisingly, this cell line rewired glutamate metabolism similarly to other tested cell lines. Therefore, the TCA cycle replenishment by glutamate and *de novo* GSH synthesis does not appear to be generally sufficient to augment the survival of leukemia cell lines under asparagine- and glutamine-depleted conditions. Interestingly, inhibition of GSH synthesis did not increase ROS levels in RS4;11 cells. Although GSH importance has been recognized for cancer cells [40], RS4;11 cells are probably not solely dependent on this most abundant intracellular antioxidant.

Glutamate addition to asparagine- and glutamine-deprived conditions shifts glucose metabolism away from fermentation to a more oxidative catabolism. Although cancer cells can respond to ROS by increasing glycolysis rate [41], it is also the pentose phosphate pathway (PPP) that controls oxidative stress via the production of NADPH [42]. In our case, ROS levels are balanced by increased glutathione biosynthesis probably accompanied with reducing agents provided by PPP. We also observed that nucleotides are preferentially synthesized from glutamate via reductive-carboxylation-originated aspartate. Since reductive carboxylation can suppress mitochondrial ROS [43], this could be another way for leukemia cells to fight glutamate-driven ROS increase.

Our study for the first time demonstrated the role of glutamate in response to ASNase treatment. Herein, we showed that extracellular glutamate can compensate for glutamine absence. Our findings are significant in the context of ASNase treatment and may have implications also for potential applications of glutamine metabolism inhibitors. These new findings point to an interaction between the use of extracellular glutamate and the need for greater GSH biosynthesis as it creates a synthetic lethal target. Moreover, our observations might shed light on why ASNase exhibits efficacy in multi-agent regimens, such as those involving ROS-inducing co-treatments like anthracyclines. New insights not only add to complexity of ASNase functioning but also have potential therapeutic implications.

3.1. Limitations of the study

The limitation of our study is that we did not explore the origin of ROS in detail. We presume ROS are mainly generated via ETC boosted by glutamate-fueled TCA. However, TCA cycle together with respiration could also be boosted by FAO. FAO was already shown to be increased upon ASNase treatment [10,44]. Furthermore, glucose contribution to ROS generation was not considered in this paper, although we have shown rewired glucose metabolism upon glutamate addition to RPMIØ, and we and others have also previously demonstrated that glucose uptake is altered upon ASNase treatment [10,44]. Therefore, we cannot exclude the influence of glucose metabolism on ROS production. Another limitation is to not directly prove increased respiration upon glutamate addition to RPMIØ. However, the incorporation of glutamate into the TCA cycle along with an increase in ROS indirectly supports the statement of induced respiration.

CRediT authorship contribution statement

Katerina Hlozkova: Writing – review & editing, Writing – original draft, Methodology, Investigation, Data curation, Conceptualization. **Maryna Vasylkivska:** Methodology, Investigation, Data curation. **Adam Boufersaoui:** Writing – review & editing, Methodology. **Bryan Marzullo:** Methodology. **Matus Kolarik:** Investigation. **Natividad Alquezar-Artieda:** Investigation. **Mehak Shaikh:** Investigation. **Nadia Fatemeh Alaei:** Investigation. **Marketa Zaliova:** Writing – review & editing, Resources. **Martina Zwyrtkova:** Investigation. **Violeta Bakardijeva-Mihaylova:** Investigation. **Meritxell Alberich-Jorda:** Methodology. **Jan Trka:** Resources, Funding acquisition. **Daniel A. Tennant:** Writing – review & editing, Methodology, Conceptualization. **Julia Starkova:** Writing – review & editing, Writing – original draft, Supervision, Funding acquisition, Data curation, Conceptualization.

Declaration of competing interest

The authors declare that they have no known competing financial interests or personal relationships that could have appeared to influence the work reported in this paper.

Acknowledgements

This work was supported by Grant Agency of Czech Republic, no: GA20-27132S, the Czech Health Research Agency, no: NU20J-03–00032, the project National Institute for Cancer Research (Programme EXCELES, ID Project No. LX22NPO5102) - Funded by the European Union - Next Generation EU and Cancer Research UK to A.B. [SEBSTF-2021\100002]. The authors acknowledge the support and resources of the Birmingham Metabolic Tracer Analysis Core.

Appendix A. Supplementary data

Supplementary data to this article can be found online at https://doi.org/10.1016/j.canlet.2024.217242.

Methods

REAGENT or RESOURCE	SOURCE	IDENTIFIER
Antibodies		
Anti-GCLC antibody [EP13475]	Abcam	Cat#ab190685
Anti-Glutathione Reductase antibody [EPR7238]	Abcam	Cat#ab124995
Anti-Glutathione Synthetase antibody [EPR6563]	Abcam	Cat#ab133592
Anti-Hu CD45 APC	EXBIO	Cat#1A-222

(*continued on next page*)

(*continued*)

REAGENT or RESOURCE	SOURCE	IDENTIFIER
BD Pharmingen™ PE Mouse Anti-Human CD73	BD Biosciences	Cat#550257
Biotin anti-mouse CD45.1 Antibody	BioLegend	Cat#110704
Goat Anti-Rabbit IgG (H + L)-HRP Conjugate #1706515	Bio-Rad	Cat#1706515
Goat Anti-Mouse IgG (H + L)-HRP Conjugate #1706516	Bio-Rad	Cat#1706516
GPX4 Antibody #52455	Cell Signaling Technology	Cat#52455S
Monoclonal Anti-β-Actin antibody produced in mouse	Sigma-Aldrich	Cat#A2228
PE/Cyanine7 anti-human CD19 Antibody	BioLegend	Cat#302216
SingleFlowEx CD10 APC-Cy™7	EXBIO	Cat#ED7168
Biological samples		
Human ALL cells from peripheral blood and bone marrow	This study	N/A
Chemicals, peptides, and recombinant proteins		
2′,7′-Dichlorodihydrofluorescein Diacetate (H_2DCFDA)	Thermo Fisher Scientific	Cat#D399
4′,6-Diamidino-2-Phenylindole, Dilactate (DAPI)	Thermo Fisher Scientific	Cat#D3571
6-Mercaptopurine monohydrate	Sigma-Aldrich	Cat#852678
Acetonitrile	Sigma-Aldrich	Cat#34851
Ammonium hydrogen carbonate	Sigma-Aldrich	Cat#5.33005
Ammonium hydroxide, 50 % v/v aq. soln.	Thermo Fisher Scientific	Cat#035574
Calcium Chloride Hexahydrate ($CaCl_2 \times 6H_2O$)	PENTA	Cat#16810-31000
Chloroform	Sigma-Aldrich	Cat#366927
Dimethyl Sulfoxide (DMSO)	Sigma-Aldrich	Cat#34869
D-Glucose (Glc)	PENTA	Cat#12020-31000
D-Glucose (U-^{13}C6, 99 %)	Cambridge Isotope Laboratories	Cat#CLM-1396-10
Ficoll® Paque Plus	Sigma-Aldrich	Cat#GE17-1440-03
Glutaric acid-d6	MedChemExpress	Cat#HY-W008820S
Hydrogen Peroxide(H_2O_2)	Sigma-Aldrich	Cat#95321
InfinityLab deactivator additive	Agilent	Cat#5191-4506
L-Asparagine Monohydrate (Asn)	Sigma-Aldrich	Cat#A7094
L-Aspartatic Acid (Asp)	Sigma-Aldrich	Cat#A7219
L-Aspartic acid ($^{13}C_4$, 99 %)	Cambridge Isotope Laboratories	Cat#CLM-1801-H-PK
L-Buthionine-Sulfoximine (BSO)	Sigma-Aldrich	Cat#B2515
L-Glutamic Acid (Glu)	Sigma-Aldrich	Cat#G8415
L- Glutamic Acid, N-Acetyl (Glutamate-^{13}C5, 97–99 %)	Cambridge Isotope Laboratories	Cat#CLM-6664-PK
L-Glutamine (Gln)	Sigma-Aldrich	Cat#G8540
Magnesium sulfate heptahydrate ($MgSO_4 \times 7H_2O$)	PENTA	Cat#25520-31000
Methanol	Sigma-Aldrich	Cat#34860
Methoxamine hydrochloride	Sigma-Aldrich	Cat#M6524
N-Acetyl-L-Cysteine (NAC)	Sigma-Aldrich	Cat#A9165
N-Ethylmaleimide (NEM)	Sigma-Aldrich	Cat#04260
N-tert-Butyldimethylsilyl-N-methyltrifluoroacetamide with 1 % tert-Butyldimethylchlorosilane	Sigma-Aldrich	Cat#00942
Potassium chloride (KCl)	PENTA	Cat#16210-31000
Pulmozyme	Genentech	N/A
Pyridine	Sigma-Aldrich	Cat#270407
Sodium Chloride (NaCl)	PENTA	Cat#16610-31000
Sodium Phosphate Monobasic Dihydrate ($NaH_2PO_4 \times 2H_2O$)	PENTA	Cat#12340-31000
Spectrila 10,000 U (ASNase)	Medac	N/A
TFB-TBOA	Tocris Bioscience	Cat#2532
Water, LC-MS Grade	Thermo Fisher Scientific	Cat#51140
Critical commercial assays		
AccuCount Blank Particles	Spherotech	Cat#ACFP-70-10
CellTiter 96 AQueous One Solution Cell Proliferation Assay	Promega	Cat#G3580
GSH/GSSG-Glo™ Assay	Promega	Cat#V6612
iScript™ Select cDNA Synthesis Kit	Bio-Rad	Cat#1708897
NextSeq 500/550 High Output Kit v2.5 (150 Cycles)	Illumina	Cat#20024907
Power SYBR™ Green PCR Master Mix	Thermo Fisher Scientific	Cat# 4368577
RNeasy Mini Kit	Qiagen	Cat#74104
SureSelect Strand - Specific RNA Library Preparation kit for Illumina	Agilent	Cat#G9691A
TruSeq Rapid PE cluster Kit-HS	Illumina	Cat#PE-402-4001
TruSeq Rapid SBS Kit-HS	Illumina	Cat#FC-402-4001
Experimental models: Cell lines		
Immortalized Human Bone Marrow Mesenchymal Cells – hTERT (MSCs)	Applied Biological Materials	T0523
JURKAT	DSMZ	ACC 282; RRID:CVCL_0065
MOLT-4	DSMZ	ACC 362; RRID:CVCL_0013
NALM-6	DSMZ	ACC 128; RRID:CVCL_0092
REH	DSMZ	ACC 22; RRID:CVCL_1650
RS4; 11	DSMZ	ACC 508; RRID:CVCL_0093

(*continued on next page*)

(*continued*)

REAGENT or RESOURCE	SOURCE	IDENTIFIER
SUP-B15	DSMZ	ACC 389; RRID:CVCL_0103
Experimental models: Organisms/strains		
NSG mouse	The Jackson Laboratory	IMSR_JAX:005557
Oligonucleotides		
SLC1A1_qF	GGTGGTGCTAGGCATTACCA	
SLC1A1_qR	TGATGAGTTTCAGCATCCGCA	
SLC1A2_qF	TCTCCCATCCACCCTGATGT	
SLC1A2_qR	GGCCACTAGCCTTAGCATCC	
SLC1A3_qF	TGCCCACTGACGACATCAC	
SLC1A3_qR	TCGTGACAAGTGCTCCACAA	
SLC1A6_qF	GGCATGAAACACAAGGGCAG	
SLC1A6_qR	GATGCCCACCAGCCTCATAA	
SLC1A7_qF	GTGGCGTACTACCTGTGGAC	
SLC1A7_qR	ATCGGCTGAGCTCATGATGG	
Software and algorithms		
GraphPad Prism	GraphPad	https://www.graphpad.com/; RRID: SCR_002798
FlowJo 10.8.1	BD	https://www.flowjo.com/; RRID:SCR_008520
MassHunter Profinder Software	Agilent	RRID:SCR_019081
Other		
Antibiotic-Antimycotic (100X)	Thermo Fisher Scientific	Cat#15240062
Fetal Bovine Serum (FBS)	Biosera	Cat#FB-1001/500
Invitrogen™ Bolt™ Bis-Tris Plus Mini Protein Gels, 4–12 %, 1.0 mm, WedgeWell™ format	Thermo Fisher Scientific	Cat#NW04127BOX
Modified (w/o Glc, Asn, Asp, Gln, Glu and Phenol Red) RPMI 1640 Medium	Thermo Fisher Scientific	N/A
Nitrocellulose Membrane, Roll, 0.45 μm, 30 cm × 3.5 m #1620115	Bio-Rad	Cat# 1620115
RPMI 1640 Medium	Thermo Fisher Scientific	Cat# 21875034
RPMI 1640 Medium, GlutaMAX™ Supplement	Thermo Fisher Scientific	Cat# 61870036
SuperSignal™ West Pico PLUS Chemiluminescent Substrate	Thermo Fisher Scientific	Cat# 34580

Cell culture

Human B cell precursor leukemia cell lines (NALM6; REH; RS4; 11; SUP-B15), T-cell leukemia cell lines (JURKAT and MOLT-4) and mesenchymal stromal cells (MSCs) were used in the study. Cell lines were obtained from the German Collection of Microorganisms and Cell Cultures (leukemia cell lines) or Applied Biological Materials (MSCs) and were negative for mycoplasma contamination.

RPMI-1640 medium with 2 mM glutamine supplemented with 10 % fetal calf serum, penicillin (100 U/mL) and streptomycin (100 μg/mL) was used for cultivation under controlled conditions (37 °C, 5 % CO_2). Cells were passaged every 3–4 days to be maintained in exponential growth phase.

Patient samples

Bone marrow samples from untreated children initially diagnosed with BCP-ALL were collected from the Czech Pediatric Hematology Centers. To be able to perform the here described experiments, only patients with a high cellularity were included. Within 24 h after aspiration, the mononuclear cells were isolated by density gradient centrifugation using Ficoll-Paque PLUS. All the samples were obtained with the informed consent of the children's parents or guardians as well as the approval of the Ethical Committee of the University Hospital Motol, Prague, Czech Republic, study no. GA20-27132S. All experiments were performed in accordance with relevant guidelines and regulations. The isolated blasts were frozen in 90 % fetal calf serum and 10 % DMSO. After thawing, the blasts were incubated for 4 h in RPMI-1640 medium with GlutaMAX™ supplemented with 50 % FBS and 100 μl of Pulmozyme.

Mouse model

NSG mice were maintained in the specific-pathogen-free (SPF) animal facility at the Institute of Molecular Genetics of the CAS. Mice were on a standard diet and 12 h light–dark cycle with free access to food and water. The experiments were approved by the Ethical Committee of the Institute of Molecular Genetics of the CAS (Prague, Czech Republic) (approval number: AVCR 7141-2022 SOV II).

Survival and proliferation of leukemia cell lines

To evaluate survival and proliferation of cell lines, they were cultivated for 72, 96 and/or 120 h in RPMIØ, RPMIØ+Asp, RPMIØ+GluA, RPMIØ+Glu and/or RPMIØ+Asp + Glu (Fig. 1F) with or without further treatment. Cells were seeded in 24-well plates at a concentration of 0.5M/mL for NALM6 and MOLT4, 0.8M/mL for REH and RS4; 11 and 3.0M/mL for SUP-B15. Then, the number of live cells was determined by absolute count on flow cytometry (BD FACSCelesta™ Cell Analyzer, BD Biosciences) using DAPI and AccuCount Blank Particles according to the manufacturer's

instructions. Data were analyzed using FlowJo software and results were expressed as absolute count of cells in single-cell, DAPI-negative population. All cell count experiments were performed in at least biological triplicates and three technical replicates.

To evaluate the cytotoxicity of BSO, MTS (dimethylthiazol carboxymethoxyphenyl sulfophenyl tetrazolium) assays were performed using a CellTiter 96 AQueous One Solution Cell Proliferation Assay according to the manufacturer's instructions. Cells were plated in sextuplicates in 96-well plates at 1.2×10^4 cells per well (2.4×10^4 in case of SUP-B15) in 100 μL of RPMI-1640 medium for 72 h. MTS assay experiments were done in three independent experiments.

Survival and proliferation of primary leukemia cells

To evaluate survival and proliferation of primary leukemia cells, they were cultivated for 120 h in RPMIØ, RPMIØ+GluA and RPMIØ+Glu (Fig. 1F) in a co-culture with MSCs. First, 20,000 MSCs were seeded in 48-well plates and after 48 h, primary cells were added at a concentration of 2.M/mL. Then, the number of live leukemia primary cells was determined by absolute count on flow cytometry (BD FACSCelesta™ Cell Analyzer, BD Biosciences) using DAPI, mCD73 and AccuCount Blank Particles according to the manufacturer's instructions. Data were analyzed using FlowJo software and results were expressed as absolute count of primary leukemia cells in single-cell, CD73-negative, DAPI-negative population. Experiments were performed in triplicates.

Determination of the intracellular ROS level

To determine intracellular ROS level, cells were cultured for 24, 48 and 72 h in hours in RPMIØ, RPMIØ+Asp, RPMIØ+GluA, RPMIØ+Glu and RPMIØ+Asp + Glu (Fig. 1F). Cells were seeded in 24-well plates at a concentration of 0.5M/mL for NALM6 and MOLT4, 0.8M/mL for REH and RS4; 11 and 3.0M/mL for SUP-B15. For ROS level measurement upon BSO treatment, cells were cultured for 24 h in full RPMI, RPMIØ and RPMIØ+Glu at a concentration of 0.8M/mL for REH and RS4; 11, 1.5M/mL for SUP-B15 and 0.5M/mL for NALM6 and MOLT4.

After culturing, cells were incubated with 20 μM H_2DCFDA in DMSO for 20 min at 37 °C in 5 % CO_2 in the dark, collected, washed with PBS and were kept on ice. Fluorescence of 2′,7′-dichlorofluorescein (DCF, oxidized form of H_2DCFDA) was measured by flow cytometry (BD FACSCelesta™ Cell Analyzer) using the fluorescein isothiocyanate (FITC) configurations. Data were analyzed using FlowJo software and ROS levels were expressed as median fluorescence of live, single-cell, FITC-positive population normalized to either RPMIØ or non-treated medium. All experiments were performed in at least three biological and three technical replicates.

Glutathione (GSH) level measurement

Total GSH level was determined using GSH/GSSG-Glo™ Assay according to the manufacturer's instructions. Luminescence was measured by column at 2 mm height with integration time of 1000 ms on SpectraMax MiniMax 300 imaging cytometer (Molecular Devices, CA, USA). Prior to measurement, cells were cultured in 6-well plate in 5 ml of RPMIØ, RPMIØ+Asp, RPMIØ+GluA, RPMIØ+Glu and RPMIØ+Asp + Glu (Fig. 1F) at the same cell concentrations as described for ROS measurement. After 24 h, cells were collected, transferred to buffer containing 111 mM NaCl, 4.7 mM KCl, 1.25 mM $CaCl_2$, 2 mM $MgSO_4$ and 1.2 mM NaH_2PO_4 (pH adjusted to 7.4) and plated in quadruplicates in 384-well plate at 5×10^4 cells per well. All GSH measurements were done in at least three independent experiments.

Western blotting

Protein lysates were prepared as previously described [45]. Proteins (30 μg per well) were resolved by NuPAGE Novex 4–12 % Bis–Tris Gels and transferred onto a nitrocellulose membrane. The membrane was probed overnight with the primary antibodies. The bound antibodies were detected with the appropriate secondary antibodies conjugated to horseradish peroxidase and visualized using an enhanced chemiluminescence reagent and documented by Uvitec (Cambridge, UK).

Metabolic tracing using GC/MS

For GC/MS tracing experiments, cells were seeded at the concentration of 1 M/ml into 24-well plates in different tracing media (specified for each experiment in the Results section) where either glucose, aspartate or glutamate was replaced by its isotopically labeled analog (either one universally labeled). After 24 h, cells were collected, washed by ice-cold saline and 500 μl of pre-chilled methanol (to −20 °C) was added. Cells were then transferred into a cold Eppendorf, 200 μl of ice-cold D6-glutaric acid (2.5 mg/ml) and 500 μl of pre-chilled chloroform (to −20 °C) were added. After shaking on ice for 10 min and centrifugation (13,000 g, 4 °C, 10 min), the polar phase was transferred to another tube and dried.

Dried down extracts were derivatized using a two-step protocol. Samples were first treated with 2 % methoxamine in pyridine (40 μl, 1 h at 60 °C) followed by addition of N-(tert-butyldimethylsilyl)-N-methyl-trifluoroacetamide, with 1 % tert-butyldimethylchlorosilane (50 μl, 1 h at 60 °C). Samples were transferred to glass vials for GC-MS analysis using an Agilent 8890 GC and 5977B MSD system. 1 μL of sample was injected in splitless mode with helium carrier gas at a rate of 1.0 ml min^{-1}. Initial GC oven temperature was held at 100 °C for 1 min before ramping to 160 °C at a rate of 10 °C min^{-1}, followed by a ramp to 200 °C at a rate of 5 °C min^{-1} and a final ramp to 320 °C at a rate of 10 °C min^{-1} with a 5 min hold. Compound detection was carried out in scan mode. Total ion counts of each metabolite were normalized to the internal standard D_6-Glutaric acid.

Metabolic tracing using LC/MS

For LC/MS tracing experiments, cells were seeded at the concentration of 1 M/ml into 24-well plates in full RPMI, RPMIØ+GluA and RPMIØ+Glu where, in all three media, glutamate was replaced by its isotopically labeled analogue $^{13}C_5$-glutamate. After 24 h, cells were collected and washed with 200 μl of ice-cold PBS/NEM solution (6.67 mM NEM in PBS). Metabolites were extracted using 100 μl of ice-cold precipitation mix (6.67 mM NEM in acetonitrile with 1 μl/ml of 1 mM mercaptopurine and 2 μg/ml of D6-glutaric acid as internal standards). After vortexing, precipitates were separated by centrifugation (13,000 g, 4 °C, 10 min), the supernatant was transferred to another tube before being stored at −80 °C. On the day of analysis samples were thawed on ice and transferred into LCMS vials.

Samples were loaded into a sample manager was maintained at 4 °C throughout. 1–10 μl of was injected into an Agilent 1290 Infinity II Liquid Chromatography system containing an Atlantis Premier BEH Z-HILIC 1.7 μm 2.1 × 150mm Column (Waters) equipped with a Vanguard precolumn. Solvent A was 20 mM Ammonium Bicarbonate (LiChropur, Sigma) with 0.1 % v/v Ammonium Hydroxide (Alfa Aesor) in 90 % Water (Honeywell)/10 % Acetonitrile (Honeywell) containing 5 μM Infinitylabs Deactivator Solution (Agilent). Solvent B was 90 % Acetonitrile/10 % Water containing 5 μM Infinitylabs Deactivator Solution. A non-linear binary gradient was used as follows: 0 min 85 % B, 2 min 85 %, 18 min 60 % B, 22 min 30 % B, 22.1 min 10 % B, 25 min 10 % B, 25.1 min 85 % B, 30 min 85 % B. The column compartment was maintained at 30° throughout. Blanks were run every 6–9 samples to monitor for metabolite carry over.

An Agilent 6546 Q-TOF was used for isotopologue measurements operating in high resolution mode with single polarity mode analysis in negative electrospray ionization. Mass calibration was performed immediately prior to each sample batch. In both modes, the drying gas was 8 l/min at 225° degrees. The nebulizer was at 30psi with a sheath gas temperature of 300° at 12 l/min. The VCap was 2000V with 500V nozzle voltage, fragmentor 125V, Skimmer 60V, Octapole RF 750V. MS1 scans were obtained at 1Hz between 50 and 1050m/z. Continuously infused reference masses of 112.985587 and 1033.988109 provided real time mass correction throughout each analytical run.

Raw data (.D) was imported into Agilent MassHunter Profinder followed by batch isotopologue extraction utilizing an in-house Personal Compound Database and Library (PCDL) containing metabolite IDs confirmed by MS/MS and pure chemical standards. A 10 ppm mass tolerance was used. Raw spectra for each potential isotopologue peak were carefully reviewed to ensure accurate representation. Data was subsequently normalized to an internal standard and cell count using in-house scripts in Excel (Microsoft).

RNA extraction, complementary DNA synthesis, and quantitative reverse transcription polymerase chain reaction

Total cellular RNA was extracted using an RNeasy mini-kit according to the manufacturer's instructions and was converted to complementary DNA using an iScript complementary DNA synthesis kit. The transcripts were detected using Power SYBR Green PCR Master Mix. PCRs were performed using a 7500 Fast Real-Time PCR system (Thermo Fisher Scientific). Expression levels were calculated using standard approach – $2^{-\Delta Ct}$. *ABL1* and *β2-microglobuline* were used as reference genes.

Whole transcriptome sequencing (RNAseq)

Sequencing libraries were prepared from total RNA (extracted from diagnostic leukemia samples) using Agilent SureSelect mRNA Strand Specific kit according to the manufacturer's instructions (Agilent Technologies, USA). High-throughput sequencing was performed on HiSeq2500 (1x50, 2x50 or 2x100 bp) or NextSeq500 (2x75 bp) using TruSeq Rapid SBS and PE Cluster kits and High Output Kit (Illumina).

Data were analyzed as described previously [46]. Counts were normalized to gene length and the R package Deseq2 [47]and vst method were used for inter-sample gene expression normalization.

NALM6-derived xenograft models

Both genders, females and males, were randomly used. Mice were 8–12 weeks old Before transplantation, all mice were irradiated, with NSG females receiving 0.8 Gy and males receiving 1 Gy. Nalm6 cells were transplanted via tail vein injection at a dose of 500,000 cells per mouse in the experimental approach. Four treatment groups were assigned to the mice. Three groups received specific drugs at designated doses three days after transplantation: TFB-TBOA at 20 mg/kg/day intraperitoneally (i.p.), L-asparaginase at 1000 U/kg/day i.p., and a control group receiving PBS at the same dose as TFB. For two weeks, three treatments were scheduled per week, followed by an additional treatment during the third week. As an additional control, two non-transplanted mice were used.

Blood analyses were conducted after two weeks of treatment to evaluate the efficacy of the administered drugs. Subsequent to an additional treatment on the 19th day, mice were sacrificed. Post-sacrifice, isolation of bone marrow and spleen was performed, followed by staining with mCD45.1, hCD45, hCD10, and hCD19 for subsequent flow cytometry analysis using the Symphony Flow Cytometer (BD Biosciences) and FlowJo software. NALM6 leukemic cells were detected as $CD45^{-}/CD10^{+}/CD19^{+}$ cells. Spleen weights were measured after isolation.

Quantification and statistical analysis

GC/MS data were analyzed using Agilent Mass Hunter software for real time analysis of data quality, before conversion to.CDF format and analysis with in-house MATLAB scripts. LC/MS data were analyzed using – Agilent MassHunter Profinder and analyzed with in-house Excel scripts.

Data are given as means of all biological and technical replicates ± SEM or ± SD, which is specified in figure legends together with sample numbers. Graphs and statistical analysis were performed using GraphPad Prism 6. Comparing two groups was performed using Student's t-test and three or more groups by one- or two-way ANOVA with Tukey's multiple comparison correction. Statistical significance is as follows: * = $p < 0.05$; ** = $p < 0.01$; *** = $p < 0.001$; **** = $p < 0.0001$.

References

[1] C.H. Pui, L.L. Robison, A.T. Look, Acute lymphoblastic leukaemia, Lancet 371 (2008) 1030–1043.
[2] C.-H. Pui, W.E. Evans, Treatment of acute lymphoblastic leukemia, N. Engl. J. Med. 354 (2006) 166–178.
[3] J. Stary, et al., Intensive chemotherapy for childhood acute lymphoblastic leukemia: results of the randomized intercontinental trial ALL IC-BFM 2002, J. Clin. Oncol. 32 (2014) 174–184.
[4] M. Schrappe, et al., Reduced intensity delayed intensification in standard-risk patients defined by minimal residual disease in childhood acute lymphoblastic leukemia: results of an international randomized trial in 1164 patients (trial AIEOP-BFM ALL 2000), Blood 128 (2016).
[5] A. Oriol, et al., Outcome after relapse of acute lymphoblastic leukemia in adult patients included in four consecutive risk-adapted trials by the PETHEMA Study Group, Haematologica 95 (2010) 589–596.
[6] B.C. Shaffer, et al., Drug resistance: still a daunting challenge to the successful treatment of AML, Drug Resist. Updates 15 (2012) 62–69.
[7] T. Oskarsson, et al., Relapsed childhood acute lymphoblastic leukemia in the Nordic countries: prognostic factors, treatment and outcome, Haematologica 101 (2016) 68.
[8] A. Pession, et al., Long-term results of a randomized trial on extended use of high dose L-asparaginase for standard risk childhood acute lymphoblastic leukemia, J. Clin. Oncol. 23 (2005) 7161–7167.

[9] Albert Moghrabi, Donna Levy, B. Asselin, et al., Results of the dana-farber cancer Institute ALL consortium protocol 95-01 for children with acute lymphoblastic leukemia, Blood 109 (2007) 896–904.
[10] I. Hermanova, et al., Pharmacological inhibition of fatty-acid oxidation synergistically enhances the effect of l-asparaginase in childhood ALL cells, Leukemia 30 (2016) 209–218.
[11] N. Alquezar-Artieda, et al., Restored biosynthetic pathways induced by MSCs serve as rescue mechanism in leukemia cells after L-asparaginase therapy, Blood. Adv. 7 (2023).
[12] J.D. Nissen, K. Pajecka, M.H. Stridh, D.M. Skytt, H.S. Waagepetersen, Dysfunctional TCA-cycle metabolism in glutamate dehydrogenase deficient astrocytes, Glia 63 (2015) 2313–2326.
[13] H.F. Alkan, J.G. Bogner-Strauss, Maintaining cytosolic aspartate levels is a major function of the TCA cycle in proliferating cells, Mol. Cell. Oncol 6 (2019).
[14] L. Xu, et al., SLC1A3 promotes gastric cancer progression via the PI3K/AKT signalling pathway, J. Cell Mol. Med. 24 (2020) 14392–14404.
[15] M. Tajan, et al., A role for p53 in the adaptation to glutamine starvation through the expression of SLC1A3, Cell Metabol. 28 (2018) 721–736.e6.
[16] C. Wang, Z. Wang, W. Liu, Z. Ai, CD133 promotes the self-renewal capacity of thyroid cancer stem cells through activation of glutamate aspartate transporter SLC1A3 expression, Biochem. Biophys. Res. Commun. 511 (2019) 87–91.
[17] J. Garcia-Bermudez, et al., Aspartate is a limiting metabolite for cancer cell proliferation under hypoxia and in tumours, Nat. Cell Biol. 20 (2018) 775–781.
[18] J. Sun, et al., SLC 1A3 contributes to L-asparaginase resistance in solid tumors, EMBO J. 38 (2019) e102147.
[19] A.A. Cluntun, M.J. Lukey, R.A. Cerione, J.W. Locasale, Glutamine metabolism in cancer: understanding the heterogeneity, Trends Cancer 3 (2017) 169.
[20] G.Y. Liao, et al., Blockage of glutamine-dependent anaplerosis affects mTORC1/2 activity and ultimately leads to cellular senescence-like response, Biol. Open 8 (2019).
[21] S. Liu, Z. Dai, D.E. Cooper, D.G. Kirsch, J.W. Locasale, Quantitative analysis of the physiological contributions of glucose to the TCA cycle, Cell Metabol. 32 (2020) 619–628.e21.
[22] D. Patel, et al., Aspartate rescues S-phase arrest caused by suppression of glutamine utilization in KRas-driven cancer cells, J. Biol. Chem. 291 (2016) 9322–9329.
[23] A.J.P.O. De Almeida, et al., ROS: basic concepts, sources, cellular signaling, and its implications in aging pathways, Oxid. Med. Cell. Longev. 2022 (2022).
[24] D.B. Zorov, M. Juhaszova, S.J. Sollott, Mitochondrial reactive oxygen species (ROS) and ROS-induced ROS release, Physiol. Rev. 94 (2014) 909–950.
[25] D.H. Kwon, et al., Protective effect of glutathione against oxidative stress-induced cytotoxicity in RAW 264.7 macrophages through activating the nuclear factor erythroid 2-related factor-2/heme oxygenase-1 pathway, Antioxidants 8 (2019) 82.
[26] M.C. Gomez-Cabrera, A. Salvador-Pascual, H. Cabo, B. Ferrando, J. Vina, Redox modulation of mitochondriogenesis in exercise. Does antioxidant supplementation blunt the benefits of exercise training? Free Radic. Biol. Med. 86 (2015) 37–46.
[27] C. le Viseur, et al., In childhood acute lymphoblastic leukemia, blasts at different stages of immunophenotypic maturation have stem cell properties, Cancer Cell 14 (2008) 47–58.
[28] W. Jiang, Y. Li, S. Zhang, G. Kong, Z. Li, Association between cellular immune response and spleen weight in mice with hepatocellular carcinoma, Oncol. Lett. 22 (2021).
[29] L. Sheng, Q. Luo, L. Chen, Special Section on New Era of Transporter Science: Unraveling the Functional Role of Orphan Transporters-Minireview Amino Acid Solute Carrier Transporters in Inflammation and Autoimmunity, Drug Metabol. Dispos. 50 (9) (2022) 1190–1192.
[30] Z.N. Ling, et al., Amino acid metabolism in health and disease, Signal Transduct. Targeted Ther. 81 (8) (2023) 1–32, 2023.
[31] L.B. Sullivan, et al., Aspartate is an endogenous metabolic limitation for tumour growth, Nat. Cell Biol. 20 (2018) 782–788.
[32] F. Meléndez-Rodríguez, et al., HIF1α suppresses tumor cell proliferation through inhibition of aspartate biosynthesis, Cell Rep. 26 (2019) 2257–2265.e4.
[33] L.B. Sullivan, et al., Supporting aspartate biosynthesis is an essential function of respiration in proliferating cells, Cell 162 (2015) 552–563.
[34] Y. Zhou, N.C. Danbolt, Glutamate as a neurotransmitter in the healthy brain, J. Neural. Transm. 121 (2014) 799.
[35] N.N. Pavlova, J. Zhu, C.B. Thompson, The hallmarks of cancer metabolism: still emerging, Cell Metabol. 34 (2022) 355–377.
[36] N.N. Pavlova, et al., As extracellular glutamine levels decline, asparagine becomes an essential amino acid, Cell Metabol. 27 (2018) 428–438.e5.
[37] R.L. Auten, J.M. Davis, Oxygen toxicity and reactive oxygen species: the devil is in the details, Pediatr. Res. 66 (2009) 121–127.
[38] E.R. Gansemer, et al., NADPH and glutathione redox link TCA cycle activity to endoplasmic reticulum homeostasis, iScience 23 (2020).
[39] D.G. Ryan, et al., Disruption of the TCA cycle reveals an ATF4-dependent integration of redox and amino acid metabolism, Elife 10 (2021).
[40] A. Bansal, M. Celeste Simon, Glutathione metabolism in cancer progression and treatment resistance, JCB (J. Cell Biol.) 217 (2018) 2291–2298.
[41] Z. Ghanbari Movahed, M. Rastegari-Pouyani, M. Hossein Mohammadi, K. Mansouri, Cancer cells change their glucose metabolism to overcome increased ROS: one step from cancer cell to cancer stem cell? Biomed. Pharmacother. 112 (2019) 108690.
[42] A. Perl, R. Hanczko, T. Telarico, Z. Oaks, S. Landas, Oxidative stress, inflammation and carcinogenesis are controlled through the pentose phosphate pathway by transaldolase, Trends Mol. Med. 17 (2011) 395–403.
[43] L. Jiang, et al., Reductive carboxylation supports redox homeostasis during anchorage-independent growth, Nature 532 (2016) 255–258.
[44] N. Alquezar-Artieda, et al., Restored biosynthetic pathways induced by MSCs serve as rescue mechanism in leukemia cells after L-asparaginase therapy, Blood Adv. 7 (10) (2023) 2228–2236.
[45] I. Hermanova, M. Zaliova, J. Trka, J. Starkova, Low expression of asparagine synthetase in lymphoid blasts precludes its role in sensitivity to L-asparaginase, Exp. Hematol. 40 (2012) 657–665.
[46] M. Zaliova, et al., Genomic landscape of pediatric B-other acute lymphoblastic leukemia in a consecutive European cohort, Haematologica 104 (2019) 1396–1406.
[47] M.I. Love, W. Huber, S. Anders, Moderated estimation of fold change and dispersion for RNA-seq data with DESeq2, Genome Biol. 15 (2014) 550.